Inorganic Material of Magnesium Nitrate Mg(NO$_3$)$_2$ Film as Q-Switcher in the C-Band Region

Noor Ummi Hazirah Hani Zalkepali[1], Muwafaq Mohammed Bakr Alsaady[1], Mustafa Mudhafar[2], Nik Noor Haryatul Eleena Nik Mahmud[1], Nur Ainnaa Mardhiah Muhammad[1], Ain Zamira Muhammad Zamri[1] and Noor Azura Awang[1]*

[1]*Photonics Devices and Sensors Research Center (PDSR), Department of Physics and Chemistry, Faculty of Applied Sciences and Technology, Universiti Tun Hussein Onn Malaysia, 84600 Pagoh, Johor, Malaysia*
[2]*Department of Pharmaceutical Chemistry, College of Pharmacy, University of Ahl Al Bayt, 56001, Karbala, Iraq*

ABSTRACT

A novel inorganic material of Magnesium Nitrate (Mg(NO$_3$)$_2$) thin film is successfully investigated in the C-band region. The Q-switcher is Mg(NO$_3$)$_2$ thin film. The solvent casting method has been applied to prepare Mg(NO$_3$)$_2$ thin film before being positioned within the fiber ferrule duo to act as a Q-switcher. Thereby, the modulation depth and the saturation intensity of the Mg(NO$_3$)$_2$ thin film exhibit at 32.40% and 0.07 MW/cm^2, respectively. It is possible to produce a steady Q-switched pulse fiber laser with a maximum pump power of 403.00 mW, a repetition rate of 72.56 kHz, and a pulse width of 3.00 µs. In addition, the tunable Q-switched pulse fiber laser is also examined using a figure-of-eight cavity design incorporating a tunable bandpass filter (TBF). Consequently, the operating wavelength is changed in the range of 1528 nm to 1552 nm, even while the pump power remains the same at 403.00 mW. During this time, the pulse width and repetition rate shifted from 2.10 µs to 4.10 µs and altered from 67.90 kHz to 35.80 kHz, respectively. Consequently, the Mg(NO$_3$)$_2$ thin film has the opportunity to be an effective saturable absorber for generating pulsed fiber lasers and can be applied in optical communications applications.

Keywords: Magnesium nitrate, pulse fiber laser, Q-switched, saturable absorber

INTRODUCTION

Numerous Q-switched pulse fiber laser applications have been widely applied in medicine, telecommunications, range findings, material processing, and sensing due to high pulse energy and peak power (Chen et al., 2013; Ahmad et al., 2015; Ahmad, Albaqawi et al., 2020). Based on the Pauli blocking principle, saturable absorbers (SA) are key elements in generating Q-switched pulse fiber lasers. In the laser cavity, high losses prevent any lasing and allow the construction of population inversion at higher energy states. When the gain is higher than the losses in the laser cavity, narrow pulse durations and high intensity of Q-switched pulse are generated (Degnan, 1995). The techniques to develop a Q-switched pulse fiber laser are active and passive. An active approach requires external modulators such as acousto-optic modulators (Cuadrado-Laborde et al., 2007; Delgado-Pinar et al., 2006) and electro-optic modulators (El-Sherif & King, 2003; Zhao et al., 2006), which have the drawbacks of high maintenance cost, bulky and expensive. On the other hand, a passive approach, by integrating a tiny piece of SA in the laser cavity, is more desirable among researchers. In addition, the advantages of using SA to generate pulse fiber lasers are their flexibility, simplicity, inexpensive design, and less consideration of dispersion, nonlinearity, and compactness.

Semiconductor saturable absorber mirrors (SESAMs) were the first discovery of SA by Keller et al. (1996). They were widely used in the 90s, exhibiting a narrow bandwidth operation, limiting the broader tunable Q-switched operation (Okhotnikov et al., 2004). The challenges of utilizing SESAMs as SAs are bandwidth limitations and fabrication complexity. Hence, this motivates the other researchers to discover other potential materials to apply as SA. Two-dimensional (2D) nanomaterials as SA have been reported, such as graphene, carbon nanotube, topological insulators (TIs), transition metal dichalcogenides (TMDs), and black phosphorus (BP). However, these materials have drawbacks, such as graphene having a low percentage modulation depth of 1.3% per layer with zero bandgaps (Sun et al., 2016) and carbon nanotube, as SA has limited bandwidth and chirality control (Sun et al., 2012).

Furthermore, the use of TIs as SA, such as bismuth selenide (Bi$_2$Se$_3$), antimony telluride (Sb$_2$Te$_3$), and bismuth telluride (Bi$_2$Te$_3$), has a problem throughout the age of dominating bulk conduction. Its susceptibility to pollution in the air environment makes operation more challenging and restricts the uses of several devices due to the unique surface conditions of TI (Kim et al., 2014). Besides that, molybdenum disulfide (MoS$_2$), tungsten disulfide (WS$_2$), molybdenum diselenide (MoSe$_2$), and tungsten diselenide (WSe$_2$) are a few examples of TMD. These substances are indirect semiconductors in bulky states made of hexagonal metal atoms sandwiched between two chalcogenide layers. They have limitations in mid-infrared applications because of their bandgap of more than 1.0 eV (Xia et al., 2014). BP is polarization-dependent and a hydrophilic substance that can easily interact with water; it

has certain limitations, including harrowing production and handling requirements (Island et al., 2015). Additionally, BP is not sufficiently stable, especially atomic BP, which is highly vulnerable to oxidative destruction in environmental settings.

Khaleel et al. (2019) have recently utilized magnesium oxide (MgO) as SA to generate a mode-locked pulse. From their study, the fixed repetition rate of 3.5 MHz is achieved at 156 mW pump power with a pulse duration of 5.6 ps and signal-to-noise ratio (SNR) of 50 dB. Moreover, the inorganic substance MgO had a direct band gap of (7.3 eV). Before now, it has been employed in several industrial, medicinal, and scientific-practical applications because of its affordable price, high breakdown field, high-temperature stability, and environmentally favorable characteristics (Płóciennik et al., 2016). Furthermore, due to its unique and alluring optical elements, such as its high optical transparency, high nonlinear optical susceptibility, strong breakdown field, and quick recovery time, MgO has recently attracted some interest in the field of ultrafast optics (Płóciennik et al., 2016; Faragl et al., 2014; Mia et al., 2017). Besides that, Morshed et al. (2017) employed magnesium diboride (MgB$_2$) to generate Q-switched by obtaining a pulse duration between 200 to 1700 ns based on a ytterbium-doped fiber laser. However, the pulse duration is changed between 200 to 1200 ns to reduce the dispersion effects after integrating the acousto-optic modulator in the cavity (Morshed et al., 2017). Thus, this motivates us to apply other inorganic materials of Mg as SA, which is integrated with the materials in the Figure-eight-cavity design to generate Q-switched.

In this research, the novel material of Mg(NO$_3$)$_2$ film is successfully fabricated and synthesized as SA by the solvent casting approach by incorporating polyvinyl alcohol (PVA). The Mg(NO$_3$)$_2$ film has modulation depth and saturation intensity of 32.40% and 0.07 MW/cm2, respectively. Furthermore, a Q-switched pulse fiber laser using Mg(NO$_3$)$_2$ film as a Q-switcher is experimentally generated by exhibiting a maximum repetition rate of 72.56 kHz and a narrow pulse width of 3.00 μs. The maximum pulse energy and average output power of the Q-switched pulse are 6.20 nJ and 0.45 mW, respectively. Moreover, at the fixed pump power of 403.00 mW, the wavelength can be modified from 1528 nm to 1552 nm due to altering the knob of TBF, which gives the tuning range of 24.00 nm.

MATERIALS AND METHODS

Preparation of Magnesium Nitrate Film

The technique of producing SA, known as the solvent-cast method, calls for using a polymer as the host material. Polymer materials come in a wide variety of forms, some of which include polymethylmethacrylate (PMMA), polyvinyl alcohol (PVA), polycarbonate, and polyimide. The fact that the solvent-cast method utilizes a one-of-a-kind drying process that dries a liquid on a surface without subjecting the material to any further mechanical or thermal stress is the primary benefit of this technique.

The material and polymer mixture must be transferred to a petri container before being utilized as SA. The mixture is allowable to dry to produce a film layer with room temperature conditions in a dry cabinet. Using a polymer composite can minimize the scattering and improve the homogeneous dispersion of the solution.

Thus, the Mg(NO$_3$)$_2$ film is prepared using solvent casting, as demonstrated in Figure 1. The Mg(NO$_3$)$_2$ was purchased from Nanochemazone with a molecular weight of 148.313 g/mol, and the purity of the material was ≥99%. Firstly, 1 g of the polyvinyl alcohol (PVA), also known as a synthetic polymer, water-soluble, and 100 ml of deionized water are mixed to dissolve the PVA by applying a magnetic stirrer in the beaker. Then, 10 mg of Mg(NO$_3$)$_2$ are dissolved in 5 ml PVA solution to create an Mg(NO$_3$)$_2$ solution. Then, the Mg(NO$_3$)$_2$

Figure 1. The solvent casting method for preparing Mg(NO$_3$)$_2$

solution undergoes ultrasonication for 90 minutes and centrifugation for 10 minutes to obtain Mg(NO$_3$)$_2$-PVA suspension with stable solution. The Mg(NO$_3$)$_2$-PVA suspension is placed in a 14.4 cm^3 petri container. Within 48 hours, the solution is permitted to dry in a dry cabinet to form Mg(NO$_3$)$_2$ film. Next, a Q-switcher is produced when a film is cut off and positioned within the fiber ferrule duo.
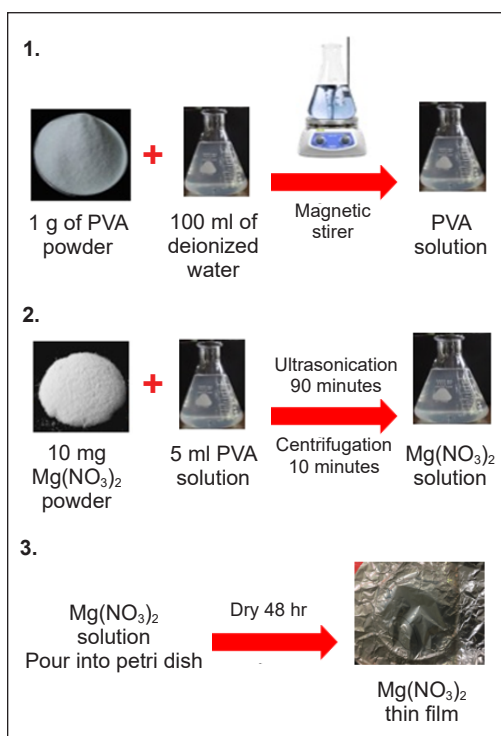
Characterization of Magnesium Nitrate Film

Figures 2(a) and (b) indicate the surface morphology of Mg(NO$_3$)$_2$ film with different magnifications of ×100 and ×10000, respectively, which is examined with the assistance of a Field Emission Scanning Electron Microscope. The surface morphology of Mg(NO$_3$)$_2$ film depicts a peak and a valley on either side, potentially arising from a small alteration in the film's thickness. Furthermore, the lack of aggregates is apparent. The Energy Dispersive X-ray exhibits the elements of magnesium, oxygen, nitrogen, and carbon, as demonstrated in Figures 2(c) and (d). The carbon parts appear during the characterization because the film is attached to the stage holder. However, the weight percentage of carbon elements is 3.1%, which is lower than magnesium, oxygen, and nitrogen, with weight percentages of 8.7%, 78.4%, and 9.8%, respectively.

The UV-Vis spectrophotometer is employed to capture the absorption spectrum of the $Mg(NO_3)_2$ film, which extends from 200 nm to 800 nm, as depicted in Figure 2(e). An evident peak signifies the occurrence of $Mg(NO_3)_2$ in the sample at 295 nm wavelength. Based on the measured absorption spectrum, the optical bandgap of $Mg(NO_3)_2$ film is recognized through the Tauc relation as Equation 1:

$$\alpha h v = A \left(h v - E_g \right)^n \qquad [1]$$

where α is the absorption coefficient, h is Planck's constant, v is the photon's frequency, A is constant, n is a type of transition; in this study, $n=2$, and E_g is the energy band gap. Determining the bandgap of a film of $Mg(NO_3)_2$ involves the extrapolation of the linear segment of the absorption edge towards the x-axis. The Tauc curve depicted in Figure 2(f) at y = 0 reveals that the optical band gap of the $Mg(NO_3)_2$ film is 4.80 eV. The analysis of the structural characteristics of $Mg(NO_3)_2$ film using Bruker-2D Phaser X-ray diffraction (XRD) in the range of 10°–80° is depicted in Figure 2(g). The main peaks are noticed, which are located at 15°, 25°, 27°, 28°, 30°, 33°, and 43.8°. The findings appear consistent with those of other studies (Sulaiman et al., 2013). The high intensities and narrow peaks of the $Mg(NO_3)_2$ film are observed in the specified peaks, and it is determined that this is because the $Mg(NO_3)_2$ film had a high crystallinity and minimum surface energy.

On the other hand, it is determined that other peaks that had been noticed are caused by the substrate as well as other defects (Oztas et al., 2012). Figure 2(h) revealed the Fourier transform infrared spectroscopy (FTIR) analysis of the $Mg(NO_3)_2$ film, conducted utilizing a Perkin Elmer FTIR Spectrometer LR 64912C; N3896 outfitted with universal Attenuated Total Reflectance (ATR) sample stage and spectrum express FTIR software V1.3.2 Perkin Elmer LX100877-1. The FTIR spectrum of the sample displays a distinctive absorption band at 3351 cm^{-1}, attributed to the O-H stretching band, N=O bending at 1645 cm^{-1}, and a mixture of N-O stretching and bending of N=O at 1351 cm^{-1}. Furthermore, the observation of bands at 819 cm^{-1} implies the existence of a bidentate type of NO^{3-} ion when interacting with Mg^{2+} (Chang & Irish, 1973).

The balance twin detector is constructed to examine the nonlinear absorption characteristics of $Mg(NO_3)_2$ films. "modulation depth" refers to the most significant degree of change in the SA absorption. It is possible to excite it by emitting light of a specific wavelength. Regarding the construction of pulse fiber lasers, modulation depth is one of the most important criteria. A reasonably large modulation depth SA can achieve a short pulse width and effective self-starting functioning due to the robust pulse-shaping capacity that the absorber possesses. An arrangement of twin detectors has a home mode mode-locked pulse laser source, attenuator, optical coupler (OC) with a ratio of 50:50, and two optical power meters (OPM), as illustrated in Figure 3(a). A mode-locked pulse is applied to measure the optical power loss of $Mg(NO_3)_2$ with operating wavelength, repetition rate, and
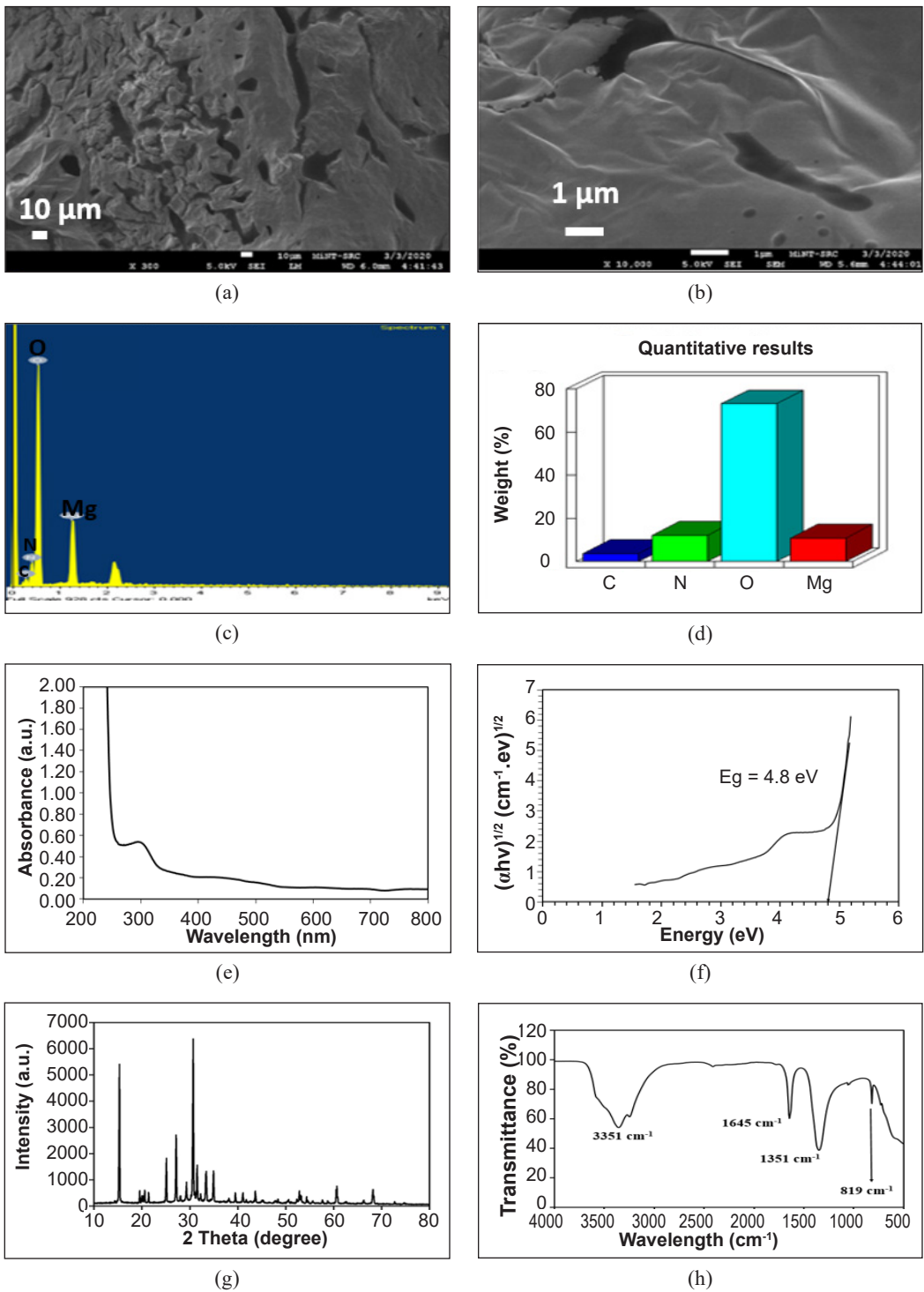
Figure 2. Mg(NO₃)₂ film: (a) and (b) the surface morphology; (c) EDX spectrum; (d) weight percentage of elements; (e) absorption spectrum; (f) energy band gap; (g) XRD pattern; and (h) FTIR spectrum
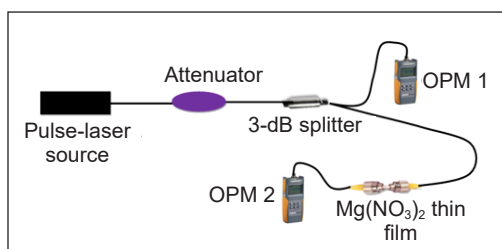
pulse width of 1570 nm, 38.73 MHz, and 640 fs, respectively. In order to generate the graph depicted in Figure 3(b), the following saturation model Equation 2 is utilized so that it can be fitted to the experimental data.

$$\alpha(I) = \frac{\alpha_s}{1 + I/I_{sat}} + \alpha_{ns} \qquad [2]$$
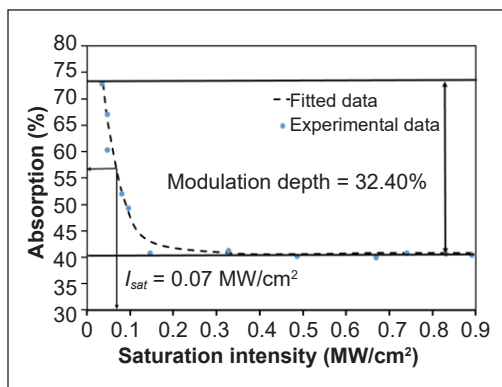
Where α is absorption, α_{ns} is non-saturable loss, α_s is saturable absorption, I is intensity, and I_{sat} is saturation intensity. The modulation depth, non-saturable absorption, and saturation intensity of $Mg(NO_3)_2$ film are 32.40%, 40.14%, and 0.07 MW/cm^2, respectively. The comparatively large modulation depth is indicative of the strong pulse-shaping capabilities of the SA, which ultimately results in short pulse duration and dependable self-starting of the Q-switched operation. Applying the SA to the experimental setup, the light photons are absorbed by electrons in the valence band, which stimulates them toward the conduction band. It is how the nonlinear behavior of the SA can be described. It is expected that the energy of any photons absorbed will be equal to the bandgap. Because the $Mg(NO_3)_2$ film has a structure consisting of energy bands, a significant

(a)

(b)

(c)

Figure 3. (a) Arrangement of twin detector method; (b) The nonlinear absorption of $Mg(NO_3)_2$ film; and (c) The illustration of insertion loss of $Mg(NO_3)_2$ film

number of electrons can be excited once the high power intensity is used. In the conduction band, the absorption of photons is significantly diminished because of the prevalence of electrons present. Figure 3(c) illustrates the insertion loss of the $Mg(NO_3)_2$ film to measure how much the signal power is diminished after passing through the SA. The insertion loss of $Mg(NO_3)_2$ film is 2.8 dB.
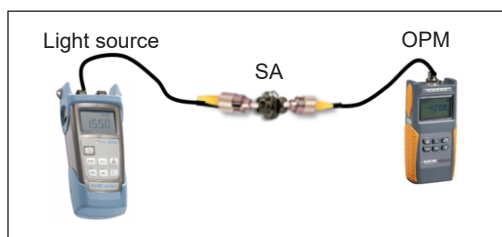
Design of Figure-of-eight

Figure 4 depicts the cavity design known as the figure-of-eight incorporating the $Mg(NO_3)_2$ film. The schematic design consists of a nonlinear amplifying mirror (NALM) (first loop)

and an optical isolator with an output optical coupler (unidirectional ring cavity) (second loop). A 50% optical coupler connects the two loops of Figure-of-eight. The first rings constructed for NALM consist of an EDF M-5 as gain media with 2 m length, wavelength division multiplexing (WDM) with a 980/1550 nm ratio, and Mg(NO$_3$)$_2$ film as SA. The small pieces of Mg(NO$_3$)$_2$ film are cut with the size of 1.74 mm^2 and attached to the fiber ferrules, then sandwiched between two fiber ferrules to form an SA. The area is measured using an optical microscope, as shown in Figure 4(b). The matching gel is dropped on the fiber ferrules to minimize light's back reflections and guarantee that the Mg(NO$_3$)$_2$ film is wholly attached to the fiber ferrule's functional area. The EDF M-5 has specifications such as absorption coefficients of 6.43 dB/m at a wavelength of 1530 nm, a coating diameter of 240.3 µm, core concentricity of 0.26 µm, a cut-off wavelength of 949 nm, a numerical aperture of 0.23, mode field diameter of 5.8 µm and fiber diameter of 124.9 µm. The propagation of the electric fields determines the laser pulse evolution in the NALM. Upon passing through the coupler, the electric fields are divided into two distinct components of varying intensities, propagating in opposite directions within the cavity (Han et al., 2020). E3 and E4 determine the electric fields circulated in the NALM in the clockwise (CW) and counterclockwise (CCW) directions, as presented in Figure 5.
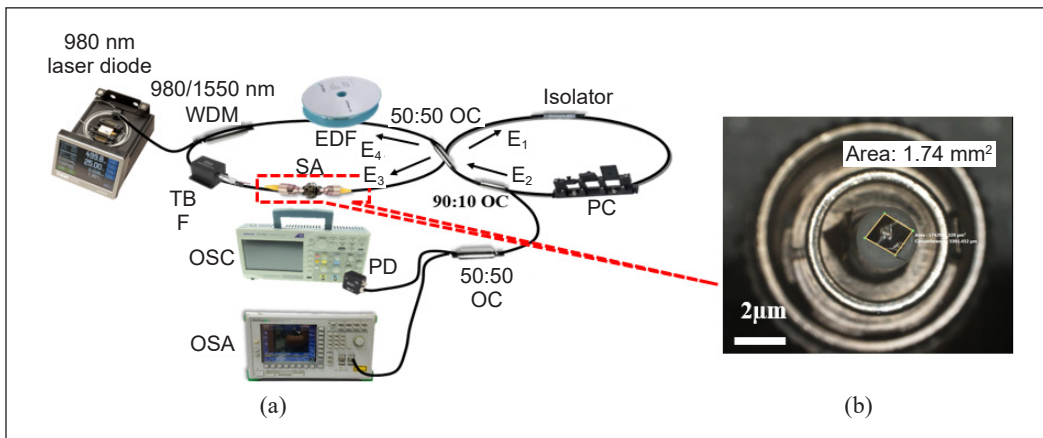

Figure 4. (a) Experimental design of tunable Q-switched pulse fiber laser using Mg(NO$_3$)$_2$ film; and (b) A small piece of SA is attached to the fiber ferrule
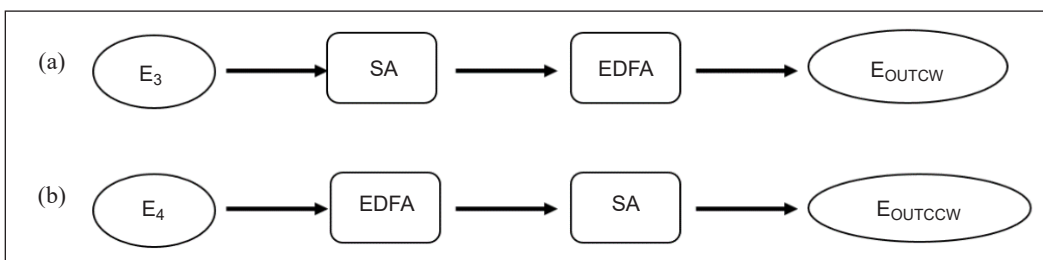

Figure 5. Schematic representation of NALM: (a) clockwise; and (b) counterclockwise direction

RESULTS AND DISCUSSION

A passive method is implemented to generate a Q-switched pulse fiber laser, and this is accomplished by incorporating a figure-of-eight cavity design into which a film of $Mg(NO_3)_2$ has been incorporated. After the $Mg(NO_3)_2$ film has been inserted, it is possible to observe the self-starting Q-switched pulse fiber laser functioning at 154.30 mW of pump power. Due to the high transmission loss impact caused by the $Mg(NO_3)_2$ embedded with PVA to produce a film, the Q-switched threshold is slightly higher than it would have been otherwise. Raising the pump power to 403.00 mW will allow for generating a steady Q-switched pulse.

The Q-switched spectrum has a center wavelength of 1553 nm, with an output power of -7.9 dBm and a resolution of 1.0 nm, as shown in Figure 6(a). Several peaks can be seen in the optical spectrum as a result of mode competition and a greater cavity length in the figure-of-eight designs. This competition mode is created due to a uniform gain broadening in EDF. Besides, in the context of electromagnetic fields in cavities, such as a figure-eight resonator, competition between multiple peaks refers to the phenomenon where different resonant modes within the cavity are vying for energy, and their frequencies influence each other. This competition arises due to the interaction and coupling between these modes, and it can lead to shifts in the resonant frequencies and changes in the mode shapes. However, it can be mitigated with the help of the inhomogeneous loss features of nonlinear polarization rotation (NPR), which causes intensity-dependent loss for various frequencies. Consequently, the equilibrium between the inhomogeneous loss generated by NPR and the mode competition effect of the EDF can result in stable multiple peak oscillations at room temperature with a uniform power distribution among the wavelengths (Feng et al., 2006).

Further increasing the pump power above 403.00 mW shows an irregular Q-switched pulse, and the pulse is stable when the pump power is between 154.30 mW and 403.00 mW. This phenomenon indicated that the $Mg(NO_3)_2$ film did not experience damage SA. It affects the unstable Q-switched caused by the oversaturation of the $Mg(NO_3)_2$ film when exposed to a high incident intensity. The process in the $Mg(NO_3)_2$ film is related to two-photon absorption, which has been initiated because of the high optical intensity. Therefore, the absorption coefficient increases as pump power continuously rises. As a result, the Q-switched procedure is unable to continue when the pump power is above 403.00 mW. The $Mg(NO_3)_2$ film in the laser cavity is eliminated to observe the condition of the Q-switched pulse. The findings indicate that only continuous waves appear on the OSC and OSA, which proves that the Q-switched pulse fiber laser can be generated with the help of $Mg(NO_3)_2$ film.

Figure 6(b) illustrates a steady Q-switched pulse train operating with a maximum pump power of 403.00 mW. The repetition rate of 72.56 kHz relates to a period of 13.78 µs and

a pulse width of 3.00 μs. Additionally, the pulse trains maintained a constant intensity distribution with no discernible variation or amplitude modulation. It demonstrates the pulse regime's stability and capacity to function at different repetition rates and pulse widths. Then, the stability of the pulse is investigated from the OSC, as illustrated in Figure 6(c). The resolution bandwidth and span from the OSC are 300 kHz and 300 Hz, respectively.

The fundamental frequency is precisely synchronized with the Q-switched pulse repetition rate of 72.56 kHz. Regarding the signal-to-noise ratio (SNR), the fundamental frequency has a value of 63.59 dB. The SNR is more significant than 50.00 dB, better or comparable to those reported by Q-switched pulse fiber laser by platinum (Yuzaile et al., 2019) and indium tin oxide (Zalkepali et al., 2019). Hence, these show that the Q-switched laser is steady, which might be appropriate for real-world uses.

When tuning the pump power, the Q-switched pulse fiber laser's repetition rate rises continuously from 35.36 kHz to 72.56 kHz. In the meantime, as seen in Figure 7(a), the pulse width dramatically declined, starting from 4.24 μs to 3.00 μs, because more photons are cycled inside the figure-of-eight cavity due to increasing pump power, saturating the Mg(NO₃)₂ film. Hence, by enhancing the modulation depth of Mg(NO₃)₂ film and shortening the fiber laser cavity design, the pulse width of the Q-switched pulse may be further reduced.

Figure 7(b) illustrates the patterns in average output power with a steady rise from 0.03 mW to 0.45 mW between working pump power of 154.30 mW and 403.00 mW. The same goes for Q-switched pulse energy, steadily increasing against the pump power from 0.88 nJ to 6.20 nJ. Both values are consistent with the Q-switched pulse
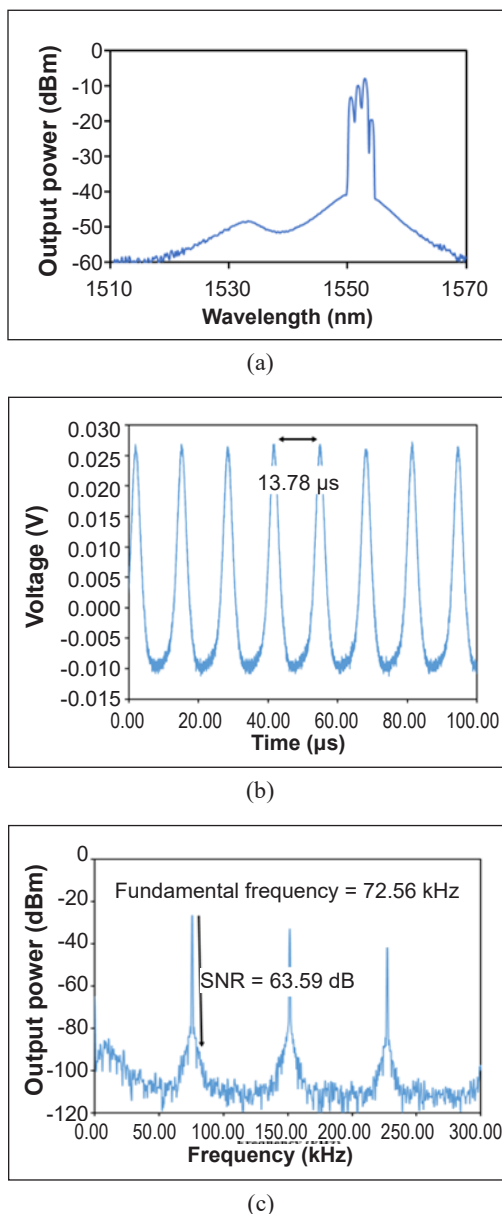
(a)

(b)

(c)

Figure 6. Q-switched pulse fiber laser: (a) optical spectrum; (b) pulse train; and (c) fundamental frequency at a pump power of 403.00 mW
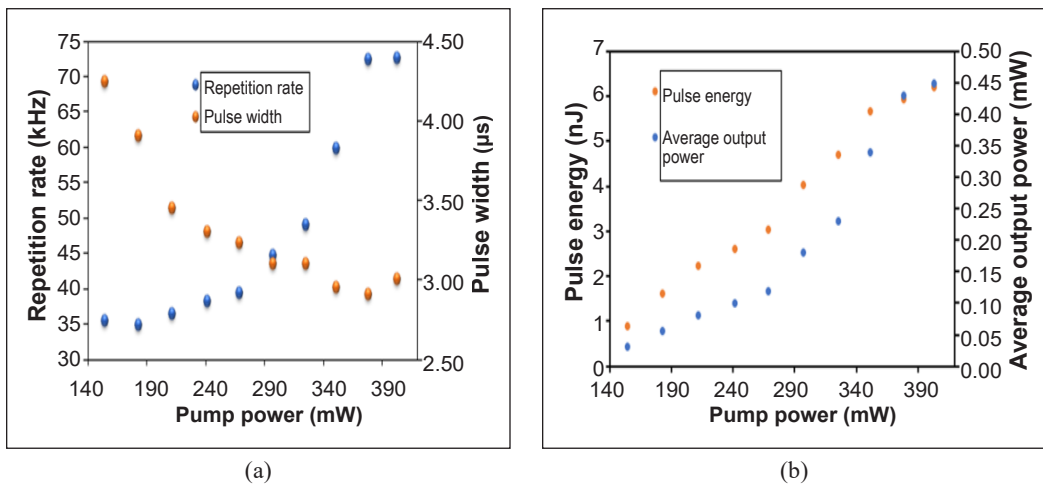
Figure 7. The relationship of: (a) repetition rate and pulse width; and (b) pulse energy and average output power by varying the pump power

fiber laser's usual properties. The proposed research shows no stable mode-locked pulse operation with this SA. These outcomes might be explained by the SA's significant inset loss or small modulation depth. For instance, the mode-locking process in the fiber laser will not be achieved when the SA cannot compensate for the output-induced disturbance or the dispersion-induced temporal broadening (Mao et al., 2016; Feng et al., 2016).

The stable Q-switched pulse at the pump power of 403.00 mW is observed for the wavelength tunability by integrating TBF inside the cavity design. The continuously tunable wavelength of the Q-switched pulse is obtained from 1528 nm to 1552 nm with a tuning range of 24 nm, as depicted in Figure 8(a). Parameters of repetition rate and pulse width are plotted, as displayed in Figure 8(b), against the lasing wavelength. The repetition rate varies significantly between 35.36 kHz and 72.56 kHz as the laser's wavelength is adjusted between 1528 and 1552 nm. It explains that the intracavity laser is more powerful, and $Mg(NO_3)_2$ film bleaching occurs more quickly under quicker population inversion/depletion at a larger-gain EDF wavelength, resulting in a higher repetition rate. The pulse width can range between 2.10 µs to 4.10 µs depending on the tuning range. Beyond the tuning wavelength, no Q-switched pulse is observed, indicating the limitation of stable wavelength tunability.

In this research, various SAs have been compared in Table 1 with Q-switched parameters. The highest repetition rate, smallest pulse width, highest pulse energy and operation, tunable wavelength, and SNR are examined and compared for the Q-switched features. Compared to MgO, MgB_2, WTe_2, Alq_3, TiO_2, and ITO, our work's SNR value is more outstanding, demonstrating that our suggested SA has superior stability and performance in producing the Q-switched pulse fiber laser. Although the WTe_2 has a more
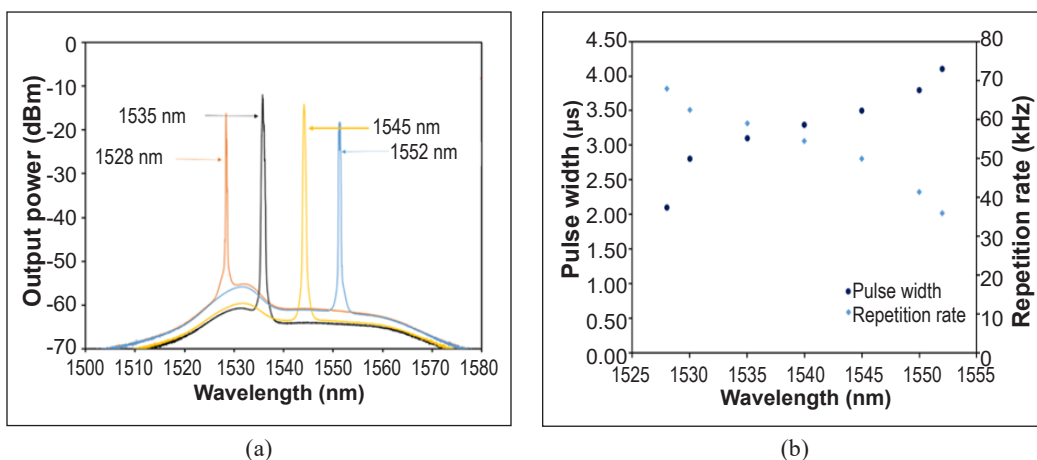
(a)	(b)

Figure 8. (a) The tunable Q-switched pulse fiber laser; and (b) the relationship of repetition rate and pulse width at a fixed pump power of 403.00 mW

significant tuning range, it still has a broader pulse width than other SA. As a result, the suggested SA effectively produces the tunable Q-switched pulse fiber laser.

The present study found that the absence of a mode-locked spectrum can be attributed to several factors within the laser cavity and the preparation of the $Mg(NO_3)_2$ as an SA. One significant contributing factor is the elongated length of the laser cavity, which poses a challenge in attaining a mode-locked spectrum. Hence, optimizing the cavity length to enable efficient operation in a mode-locked regime is crucial. Furthermore, the initial presence of high cavity loss poses a challenge in achieving the necessary power level for successful mode-locked operation. The potential cause of this cavity loss can be attributed to various factors, including the characteristics of the SA itself, the fiber ferrule adapter, and other components incorporated into the figure-eight cavity design. The successful attainment of mode-locked operation necessitates the synchronization of phases across numerous longitudinal modes.

CONCLUSION

In conclusion, a novel inorganic $Mg(NO_3)_2$ film material is successfully investigated as a Q-switcher. The $Mg(NO_3)_2$ film is synthesized using solvent casting. Based on the analysis of the nonlinear absorption, the modulation depth is 32.40%, and the saturation intensity is 0.07 MW/cm². The higher repetition rate of 72.56 kHz is performed at a stable Q-switched pulse fiber laser using 403.00 mW pump power, displaying the shortest pulse of 3.00 μs. Furthermore, incorporating TBF in a figure-of-eight cavity design at 403.00 mW pump power allows the Q-switched pulse fiber laser wavelength to be adjusted from 1528 nm to 1552 nm. Consequently, it provides tuning results for a pulse width of 2.10 μs to 4.10 μs. Meanwhile, the repetition rate ranges from 67.90 kHz to 35.80 kHz. Therefore, the

Table 1
The comparison of previous saturable absorbers with this work

Types of SA	Modulation depth (%)	Saturation Intensity (MW/cm^2)	Operational / Tunable Wavelength (nm)	Tuning range (nm)	Repetition rate (kHz)	Pulse width (µs)	Pulse energy (nJ)	Average output power (mW)	SNR (dB)	Ref.
MgO	32.4	16.00	1569.1/NA	NA	350000.00	0.0000056	2.17	3.5	50.00	Khaleel et al., 2019
MgB$_2$	NA	NA	1070/NA	NA	50.00	0.92	NA	NA	NA	Morshed et al., 2017
WTe$_2$	20.0	0.025	1494/1459-1513	54	36.50	3.70	16.5	0.60	42.00	Ahmad, Ismail et al., 2020
Alq$_3$	8.1	3.000	1563.3/1520-1563.3	43.3	71.00	2.12	37.0	2.63	53.00	Salam et al., 2021
TiO$_2$	19.1	0.040	1532-1570	38	83.30	0.08	0.41	NA	45.00	Ahmad et al., 2019
ITO	NA	NA	1562.07/1540-1570	30	94.34	3.22	30.29	2.86	58.93	Zalkepali et al., 2021
Mg(NO$_3$)$_2$	1.5	0.450	1562.37 / 1528-1552	24	72.56	3.00	6.20	0.45	63.59	This work

Mg(NO$_3$)$_2$ film may have the opportunity to be implemented in an application involving optical communications. Furthermore, the ultrashort pulse fiber laser can be obtained by optimizing the preparation of Mg(NO$_3$)$_2$ film and figure-of-eight cavity design.

ACKNOWLEDGEMENTS

REFERENCES

Ahmad, H., Albaqawi, H.S., Yusoff, N., Bayang, L., Kadir, M. Z. B. A., & Yi, C.W. (2020). Tunable passively Q-switched erbium-doped fiber laser based on Ti$_3$C$_2$Tx MXene as saturable absorber. *Optical Fiber Technology, 58*, Article 102287. https://doi.org/10.1016/jyofte.2020.102287

Ahmad, H., Ismail, N. N., Aidit, S. N., Yusoff, N., & Zulkifli, M. Z. (2020). Tunable S+/S band Q-switched thulium-doped fluoride fiber laser using tungsten ditelluride (WTe2). *Results in Physics, 17*, Article 103124. https://doi.org/10.1016/j.rinp.2020.103124

Ahmad, H., Reduan, S. A., Ruslan, N. E., Lee, C. S. J., Zulkifli, M. Z., & Thambiratnam, K. (2019). Tunable Q-switched erbium-doped fiber laser in the C-band region using nanoparticles (TiO$_2$). *Optics Communications, 435*, 283-288. https://doi.org/10.1016/j.optcom.2018.11.035

Ahmad, H., Soltanian, M.R.K., Narimani, L., Amiri, I.S., Khodaei, A., & Harun, S.W. (2015). Tunable S-band Q-switched fiber laser using Bi$_2$Se$_3$ as the saturable absorber. *IEEE Photonics Journal, 7*(3), 1-8. https:// doi. org/ 10.1109/JPHOT.2015.2433020

Chang, T. G., & Irish, D. E. (1973). Raman and infrared spectra study of magnesium nitrate-water systems. *The Journal of Physical Chemistry, 77*(1), 52-57. https://doi.org/10.1021/j100620a011

Chen, Y., Zhao, C., Chen, S., Du, J., Tang, P., Jiang, G., Zhang, H., Wen, S., & Tang, D. (2013). Large energy, wavelength widely tunable, topological insulator Q-switched erbium-doped fiber laser. *IEEE Journal of Selected Topics in Quantum Electronics, 20*(5), 315-322. https://doi. org/10.1109/JSTQE.2013.2295196

Cuadrado-Laborde, C., Delgado-Pinar, M., Torres-Peiró, S., Díez, A. & Andrés, M.V. (2007). Q-switched all-fibre laser using a fibre-optic resonant acousto-optic modulator. *Optics Communications, 274*(2), 407-411. https://doi.org/10.1016/j.optcom.2007.02.032

Degnan, J. J. (1995). Optimization of passively Q-switched lasers. *IEEE Journal of Quantum Electronics, 31*(11), 1890-1901. https://doi.org/10.1109/3.469267

Delgado-Pinar, M., Zalvidea, D., Diez, A., Pérez-Millán, P., & Andrés, M. V. (2006). Q-switching of an all-fiber laser by acousto-optic modulation of a fiber Bragg grating. *Optics Express, 14*(3), 1106-1112. https://doi. org/10.1364/OE.14.001106

El-Sherif, A. F., & King, T. A. (2003). High-energy, high-brightness Q-switched Tm^{3+}-doped fiber laser using an electro-optic modulator. *Optics Communications, 218*(4-6), 337-344. https://doi.org/10.1016/s0030-4018(03)01200-8

Faragl, M. A., El-Okr, M., Mahani, R. M., Turky, G. M., & Afify, H. H. (2014). Investigation of dielectric and optical properties of MgO thin films. *International Journal of Advancement in Engineering, Technology and Computer Sciences, 1*(1), 1-9.

Feng, T., Mao, D., Cui, X., Li, M., Song, K., Jiang, B., Lu, H., & Quan, W. (2016). A filmy black-phosphorus polyimide saturable absorber for Q-switched operation in an erbium-doped fiber laser. *Materials, 9*(11), Article 917. https://doi.org/10.3390/ma9110917

Feng, X., Tam, H. Y., & Wai, P. K. A. (2006). Stable and uniform multiwavelength erbium-doped fiber laser using nonlinear polarization rotation. *Optics Express, 14*(18), 8205-8210. https://doi.org/10.1364/OE.14.008205

Han, Y., Guo, Y., Gao, B., Ma, C., Zhang, R., & Zhang, H. (2020). Generation, optimization, and application of ultrashort femtosecond pulse in mode-locked fiber lasers. *Progress in Quantum Electronics, 71*, Article 100264. https://doi.org/10.1016/j.pquantelec.2020.100264

Island, J. O., Steele, G. A., van der Zant, H. S., & Castellanos-Gomez, A. (2015). Environmental instability of few-layer black phosphorus. *2D Materials, 2*(1), Article 011002. https://doi.org/10.1088/2053-1583/2/1/011002

Keller, U., Weingarten, K. J., Kartner, F. X., Kopf, D., Braun, B., Jung, I. D., Fluck, R., Honninger, C., Matuschek, N., & Der Au, J. A. (1996). Semiconductor saturable absorber mirrors (SESAM's) for femtosecond to nanosecond pulse generation in solid-state lasers. *IEEE Journal of selected topics in Quantum Electronics, 2*(3), 435-453. https://doi.org/10.1109/2944.571743

Khaleel, W. A., Sadeq, S. A., Alani, I. A. M., & Ahmed, M. H. M. (2019). Magnesium oxide (MgO) thin film as saturable absorber for passively mode locked erbium-doped fiber laser. *Optics & Laser Technology, 115*, 331-336. https://doi.org/10.1016/j.optlastec.2019.02.042

Kim, N., Lee, P., Kim, Y., Kim, J. S., Kim, Y., Noh, D. Y., Yu, S. U., Chung, J., & Kim, K. S. (2014). Persistent topological surface state at the interface of Bi_2Se_3 film grown on patterned graphene. *ACS Nano, 8*(2), 1154-1160. https://doi.org/10.1021/nn405503k

Mao, D., She, X., Du, B., Yang, D., Zhang, W., Song, K., Cui, X., Jiang, B., Peng, T., & Zhao, J. (2016). Erbium-doped fiber laser passively mode locked with few-layer $WSe_2/MoSe_2$ nanosheets. *Scientific Reports, 6*(1), Article 23583. https://doi.org/10.1038/srep23583

Mia, M. N. H., Pervez, M. F., Hossain, M. K., Rahman, M. R., Uddin, M. J., Al Mashud, M. A., Ghosh, H. K., & Hoq, M. (2017). Influence of Mg content on tailoring optical bandgap of Mg-doped ZnO thin film prepared by sol-gel method. *Results in physics, 7*, 2683-2691. https://doi.org/10.1016/j.rinp.2017.07.047

Morshed, M., Hattori, H. T., Haque, A., & Olbricht, B. C. (2017). Magnesium diboride (MgB_2) as a saturable absorber for a ytterbium-doped Q-switched fiber laser. *Applied Optics, 56*(27), 7611-7617. https://doi.org/10.1364/AO.56.007611

Okhotnikov, O., Grudinin, A., & Pessa, M. (2004). Ultra-fast fibre laser systems based on SESAM technology: New horizons and applications. *New Journal of Physics, 6*(1), Article 177. https://doi.org/10.1088/1367-2630/6/1/177

Oztas, M., Bedýr, M., Sur, S., & Öztürk, Z. (2012). Influence of an aqueous/ethanolic solution on the structural and electrical properties of polycrystalline ZnS films. *Chalcogenide Letters, 9*(6), 249-256.

Płóciennik, P., Guichaoua, D., Zawadzka, A., Korcala, A., Strzelecki, J., Trzaska, P., & Sahraoui, B. (2016). Optical properties of MgO thin films grown by laser ablation technique. *Optical and Quantum Electronics, 48*, 1-12. https://doi.org/10.1007/s11082-016-0536-8

Salam, S., Nizamani, B., Yasin, M., & Harun, S. W. (2021). C-band tunable Q-switched fiber laser based on Alq₃ as a saturable absorber. *Results in Optics, 2*, Article 100036. https://doi.org/10.1016/j.rio.2020.100036

Sulaiman, M., Rahman, A. A., & Mohamed, N. S. (2013). Structural, thermal and conductivity studies of magnesium nitrate–alumina composite solid electrolytes prepared via sol-gel method. *International Journal of Electrochemical Science, 8*, 6647-6655.

Sun, Z., Hasan, T., & Ferrari, A. C. (2012). Ultrafast lasers mode-locked by nanotubes and graphene. *Physica E: Low-dimensional Systems and Nanostructures, 44*(6), 1082-1091. https://doi.org/10.1016/j.physe.2012.01.012

Sun, Z., Martinez, A., & Wang, F. (2016). Optical modulators with 2D layered materials. *Nature Photonics, 10*(4), 227-238. https://doi.org/10.1038/nphoton.2016.15

Xia, F., Wang, H., & Jia, Y. (2014). Rediscovering black phosphorus as an anisotropic layered material for optoelectronics and electronics. *Nature Communications, 5*(1), Article 4458. https://doi.org/10.1038/ncomms5458

Yuzaile, Y. R., Awang, N. A., Zalkepali, N. U. H. H., Zakaria, Z., Latif, A. A., Azmi, A. N., & Hadi, F. A. (2019). Pulse compression in Q-switched fiber laser by using platinum as saturable absorber. *Optik, 179*, 977-985. https://doi.org/10.1016/j.ijleo.2018.11.057

Zalkepali, N. U. H. H., Awang, N. A., Yuzaile, Y. R., Zakaria, Z., Latif, A. A., Ali, A. H., & Mahmud, N. N. H. E. N. (2019). Indium tin oxide thin film based saturable absorber for Q-switching in C-band region. *Journal of Physics: Conference Series IOP Publishing, 1371*(1), Article 012018. https://doi.org/10.1088/1742-6596/1371/1/012018

Zalkepali, N. U. H. H., Awang, N. A., Yuzaile, Y. R., Zakaria, Z., Latif, A. A., Ali, A. H., & Mahmud, N. N. H. E. (2021). Tunable indium tin oxide thin film as saturable absorber for generation of passively Q-switched pulse erbium-doped fiber laser. *Indian Journal of Physics, 95*, 733-739. https://doi.org/10.1007/s12648-020-01738-y

Zhao, S., Zhao, J., Li, G., Yang, K., Sun, Y., Li, D., An, J., Wang, J. & Li, M. (2006). Doubly Q-switched laser with electric-optic modulator and GaAs saturable absorber. *Laser Physics Letters, 3*(10), 471-473. https://doi.org/ 10.1002/lapl.200610038